JACS
JOURNAL OF THE AMERICAN CHEMICAL SOCIETY

ARTICLE

pubs.acs.org/JACS

# A New Structural Model of A$\beta_{40}$ Fibrils

Ivano Bertini,[*,†,‡,§] Leonardo Gonnelli,[†] Claudio Luchinat,[*,†,‡] Jiafei Mao,[†,§] and Antonella Nesi[†]

[†]Magnetic Resonance Center (CERM), University of Florence, Via L. Sacconi 6, 50019 Sesto Fiorentino, Italy

[‡]Department of Chemistry "Ugo Shiff", University of Florence, Via della Lastruccia 3, 50019 Sesto Fiorentino, Italy

[§]Fondazione Farmacogenomica FiorGen onlus, Via L. Sacconi 6, 50019 Sesto Fiorentino, Italy

Supporting Information

**ABSTRACT:** The amyloid fibrils of beta-amyloid (A$\beta$) peptides play important roles in the pathology of Alzheimer's disease. Comprehensive solid-state NMR (SSNMR) structural studies on uniformly isotope-labeled A$\beta$ assemblies have been hampered for a long time by sample heterogeneity and low spectral resolution. In this work, SSNMR studies on well-ordered fibril samples of A$\beta_{40}$ with an additional N-terminal methionine provide high-resolution spectra which lead to an accurate structural model. The fibrils studied here carry distinct structural features compared to previous reports. The inter-$\beta$-strand contacts within the U-shaped $\beta$-strand-turn-$\beta$-strand motif are shifted, the N-terminal region adopts a $\beta$-conformation, and new inter-monomer contacts occur at the protofilament interface. The revealed structural diversity in A$\beta$ fibrils points to a complex picture of A$\beta$ fibrillation.

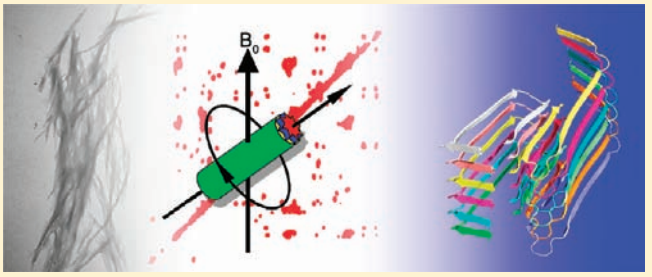


## INTRODUCTION

Beta-amyloids (A$\beta$) are a group of peptides (36−45 residues) produced by the $\beta$- and $\gamma$-secretase-dependent cleavage of amyloid precursor protein.[1] The amyloidic senile plaques, which are rich in amyloidal fibrils formed by A$\beta$ peptides, constitute one of the pathological hallmarks and a popular drug target for Alzheimer's disease (AD), a neurodegenerative disease characterized by dementia and other irreversible neural disorders through the progressive lesion of multiple brain regions.[2,3] In addition, Down's syndrome, a genetic disease leading to intellectual disability and physical growth impairment, is also linked to toxic A$\beta$ species.[4] *In vitro* A$\beta$ peptides self-assemble into a variety of amyloidal aggregates such as oligomers, transmembrane pores, protofibrils, and mature fibrils with distinct morphologies.

Given the importance of A$\beta$ amyloid species in AD, the structural characterization of these aggregates has attracted the attention of many researchers.[5−17] Previous structural studies based on solid-state nuclear magnetic resonance (SSNMR) and electron microscopy (EM) have identified diverse morphologies and structures of A$\beta$ fibrils. For example, by combining SSNMR and EM, different symmetric organization of protofilaments has been found in A$\beta_{40}$ fibrils within distinct morphologies ("twisted pairs" and "striated ribbons").[18,19] Recent cryo-EM studies found very complex polymorphism of A$\beta_{40}$ fibrils characterized by various size, cross section, and width modulation,[9,20] many of which seem very different from those of fibrils studied by SSNMR.[21] Collectively, these results point to a complex picture of polymorphism of A$\beta$ fibrils. Indeed, polymorphism is a general phenomenon which has been observed on various amyloids.[22−24] The polymorphism/structure diversity of A$\beta$ fibrils widely observed *in vitro* and *in vivo* could complicate their pathological effects.[6,25−27] Therefore, for a comprehensive understanding of the molecular basis of AD, detailed structural investigations are needed on A$\beta$ fibrils with different morphologies and formed under a variety of conditions. In the past decade, SSNMR has achieved encouraging progress in providing site-specific structural and functional information on biomacromolecules[28] in different forms,[29−34] and in particular in amyloidic aggregates.[35−42] Studies of A$\beta$ assemblies by SSNMR are usually complicated by polymorphism, and even by the concomitant structural disorder that may exist in certain aggregates. In addition, SSNMR spectra of A$\beta$ aggregates often show relatively large line widths (1.5−2.5 ppm)[43] that could also originate in part from the structural heterogeneity of the samples. This limitation has been overcome by taking advantage of programmed isotopic labeling schemes, which however hamper full structural analysis by SSNMR.[6,7,14,18,19,26,44−49]

In this work, we pursue comprehensive and site-specific structural investigation of mature, uniformly [$^{13}$C,$^{15}$N]-enriched A$\beta_{40}$ (with one exogenous N-terminal methionine residue, Met0) fibrils through SSNMR. A$\beta_{40}$ was selected for this study because it is one of the main A$\beta$ species in brain interstitial fluid and senile plaques,[50−52] and the available structural and functional data on this system can ensure comparative data interpretation. The high quality of the SSNMR spectra obtained in this work indicates high molecular homogeneity of the fibrils. This permits a more complete characterization of the A$\beta_{40}$ folding in this fibrillar form. A novel structural model of A$\beta_{40}$

**Received:** April 19, 2011
**Published:** September 01, 2011

fibrils bearing several unique structural features is proposed. Comparative analysis of the results from the current work and previous reports makes it possible to obtain insights into the molecular basis of distinct types of structural diversity in A$\beta$ fibrils. This work offers new clues toward uncovering biophysical, pathological, and biomedical issues related to A$\beta$.

## MATERIALS AND METHODS

**Expression, Purification, and Fibrillation of A$\beta_{40}$ Peptide.** The complementary DNA of A$\beta_{40}$ was cloned in the pET3a vector using the *Nde*I and *Bam*HI restriction enzymes. The peptide was expressed in the BL21 (DE3)pLys *Escherichia coli* strain. The expressed peptide contains Met0 due to the translation of start codon. The cells transformed with the A$\beta_{40}$ expression plasmid were grown in rich medium at 39 °C until $OD_{600}$ reached 1.0. The cells were then centrifuged and resuspended in M9 minimal medium enriched with $(^{15}NH_4)_2SO_4$ (1 g/L) and [U-$^{13}$C]glucose (3 g/L). Peptide expression was induced with 1.2 mM isopropyl $\beta$-D-1-thiogalactopyranoside, and cells were harvested after 3 h incubation at 39 °C. The peptide was purified as reported[53−55] with some modifications. The inclusion bodies were first solubilized with 8 M urea and then purified by ion exchange chromatography. The A$\beta_{40}$ fraction was eluted with 125 mM NaCl. Guanidinium chloride was then added to the solution to reach the final concentration of 6 M. The peptide was concentrated, and the monomeric A$\beta_{40}$ fraction was isolated by size exclusion chromatography in 50 mM ammonium acetate (pH 8.5). The final yield was about 10−15 mg/L.

For the SSNMR studies, 100 $\mu$M A$\beta_{40}$ in 50 mM ammonium acetate (pH 8.5) was incubated at 37 °C under shaking (950 rpm) for 4 weeks. Fibrils were collected by ultracentrifugation at 60 000 rpm ($\sim 2.65 \times 10^5 g$) and 4 °C for 24 h. The pellet was washed with fresh, cold ultrapure water (Millipore) three times (1 mL each time), and then ∼10 mg of wet material was packed into a 3.2 mm $ZrO_2$ magic angle spinning (MAS) rotor at 4 °C. The fibril samples were kept fully hydrated during all steps.

For transmission electron microscopy (TEM) tests, a suspension of A$\beta_{40}$ fibrils was dropped and dried on a Cu grid covered by carbon film. The fibrils were then stained in freshly prepared aqueous uranyl acetate solution for 20 min. After that, the grid was rinsed gently using ultrapure water for 1 min and dried again. Bright-field TEM images were collected on a Philips CM12 microscope operating at 80 kV.

**SSNMR Experiments.** $^{13}$C−$^{13}$C 2D dipolar-assisted rotational resonance (DARR, with <100 ms mixing time),[56,57] $^{15}$N−$^{13}$C 2D proton-assisted insensitive nuclei cross-polarization (PAIN-CP),[58,59] NCA, NCO, NCACX (3D), NCOCX (3D), and CANCO (3D) experiments were performed on a Bruker Avance III 850 MHz wide-bore spectrometer (20.0 T, 213.7 MHz $^{13}$C Larmor frequency) equipped with a 3.2 mm DVT MAS probe head in triple-resonance mode. The MAS frequency ($\omega_r/2\pi$) was 14.0 kHz (±2 Hz) during most of these experiments, except in the PAIN-CP experiment, for which a MAS frequency of 19.0 (±3 Hz) was used. During the 2D $^{13}$C−$^{13}$C DARR mixing time, a radio frequency (RF) pulse of constant strength equal to $\omega_r/2\pi$ was applied on the $^1$H channel. The NCA, NCO, NCACX, NCOCX, and CANCO experiments were carried out using the standard pulse sequences as reported in the literature.[60−63] The $^1$H heteronuclear decoupling was turned off during the $^{15}$N−$^{13}$C′ cross-polarization following a recently published method.[64] PAIN-CP was performed by irradiating the sample with constant RF strengths around $2.5\omega_r/2\pi$ on all $^1$H, $^{13}$C, and $^{15}$N channels for 10 ms. The $^{13}$C carrier frequency was set to 40 ppm during PAIN-CP. The RF strength and the contact time of PAIN-CP were carefully optimized, aiming at maximizing the signal intensity in the $^{13}$C chemical shift range of 0−40 ppm. 2D $^{13}$C−$^{13}$C proton-driven spin diffusion (PDSD)[65]/DARR correlation spectra with mixing times >100 ms were recorded on a Bruker Avance 700 MHz wide-bore instrument (16.4 T, 176.0 MHz $^{13}$C Larmor frequency) equipped with a 3.2 mm DVT probe head in the double-resonance mode. For these experiments, the MAS frequency was stabilized at 11.5 kHz (±2 Hz). During the experiments carried out using the 3.2 mm probe heads, the sample was cooled by a dry, cold air flow (>1470 L/h) generated by a BCU unit (BCU-Xtreme or BCU-05), and the effective sample temperature during the experiments was estimated to be ∼10 °C.

The spin-state-selection ($S^3E$) NCO experiment[66] and proton-assisted recoupling (PAR)[67,68] were performed on a Bruker Avance III 850 MHz wide-bore spectrometer equipped with a 1.3 mm DVT probe head in the triple-resonance mode. During these experiments, the sample was spun at 50.0 kHz (±5 Hz) and kept at ∼20 °C by a strong air flow (1735 L/h) generated by a BCU-Xtreme unit. $^{15}$N−$^{13}$C′ double CP (2.8 ms) in the $S^3E$ NCO experiment was performed by applying a $^{15}$N RF pulse about 26 kHz and a tangential amplitude modulation $^{13}$C RF pulse at 29.3 kHz. The length of the Q3 Gaussian-shaped pulse cascades used in the $S^3E$ scheme was set to 750 $\mu$s. The PAR mixing was performed by applying a $^{13}$C RF pulse at 58.3 kHz ($1.17\omega_r/2\pi$) and a $^1$H RF pulse at 10.6 kHz ($0.21\ \omega_r/2\pi$) for 10 or 15 ms. The 90° $^1$H and $^{13}$C pulses used for calculating these RF strength in the PAR mixing were obtained consistently through direct measurements and back calculation from several optimized double-quantum CP conditions at 50 kHz MAS. The RF strengths used in PAR mixing were optimized through maximizing the intensity of signals in 1D mode (evolution time was set to zero). A low-power TPPM decoupling at 20.0 kHz ($0.40\omega_r/2\pi$) was applied during the evolution and the acquisition time in the experiments performed at 50 kHz MAS.

More details on the parameters used for the SSNMR experiments are reported in the Supporting Information.

**SSNMR Data Analysis and Structural Modeling.** The sequential assignment and the analysis of DARR, PDSD, PAR, and PAIN spectra was conducted using the CARA program[69] and the SPARKY program,[70] respectively. We found that the previously published assignments on A$\beta$ fibrils[6,7,14,19,44,48] as well as the spectral patterns generated from them could not be directly used as references for assigning the present spectra, which is obviously due to structural differences. The sequential assignment started from the identification of consecutive residues Ile31 and Ile32, the side-chain signals of which could be easily distinguished. From Ile31 the assignment was extended using the following protocol. First, the spin system of a certain residue ($i$) was identified on the NCACX spectrum (N($i$)−C$\alpha$($i$)−CX($i$)). Then the sequential link between the current ($i$) residue and the previous ($i-1$) residue was searched for in the CANCO spectrum (C$\alpha$($i$)−N($i$)−C′($i-1$)). After that the spin system of residue ($i-1$) was identified in the NCOCX spectrum (N($i$)−C′($i-1$)−CX($i-1$)) and in the NCACX spectrum (N($i-1$)−C$\alpha$($i-1$)−CX($i-1$)). These steps were repeated in a sequential fashion. The extension of the assignment from Ile32 to the C-terminus was done in a similar way. Some other unique sites, e.g., Arg5 (the only Arg in the sequence) and the Gly37-Gly38 pair (the only Gly-Gly pair in the sequence), could be identified independently and were used to verify the assignment. The $^{13}$C and $^{15}$N chemical shifts were indirectly referenced to trimethylsilyl propionate (TSP) and liquid $NH_3$, respectively. The secondary chemical shifts ($\Delta\delta$) were calculated following the definition in ref 71. The secondary structural probability was calculated by the TALOS+ program.[72]

For model building, the $\beta$1 and $\beta$2 strands were based on the secondary structure predicted by the TALOS+ program. Since the parallel registry of the $\beta$1 and $\beta$2 strands is the only one consistent with the present spectra (see Results section), we then duplicated the $\beta$1 and $\beta$2 strands along the direction of the backbone N−H and C═O bonds using a typical interstrand distance of 4.7 Å, to construct $\beta$-sheets. These $\beta$-sheets could contain an arbitrary number of strands. In practice, $\beta$1- and $\beta$2-sheets containing six $\beta$-strands each were used. The $\beta$1- and $\beta$2-sheets constructed as described above were then docked to one

another by the HADDOCK program[73,74] using the experimental long-range $\beta1-\beta2$ restraints. HADDOCK calculations were performed on the WeNMR GRID (http://www.wenmr.eu/) through the HADDOCK webserver Expert interface.[75] All observed long-range contacts as well as the subset of contacts used as restraints for HADDOCK calculations (unambiguous contacts obtained using relatively short mixing times) are listed in Table S2. The lower distance cutoff in the HADDOCK calculations was set to 3.0 Å, and the upper distance cutoff was set to 6.0 Å for the short mixing contacts (100−200 ms) and to 8.0 Å (≥400 ms) for the long mixing contacts. The charges on the N- and C-termini of the $\beta1$-strands and on the N-termini of the $\beta2$-strands were not included in the calculations in order to prevent electrostatic interactions, which do not exist when the two $\beta$-strands are linked by a turn region. The histidine protonation states were automatically determined by the WHATIF program which is embedded in the HADDOCK server on the WeNMR GRID. The number of structures for rigid body docking was set to 1000. Semi-flexible refinement was enabled on both $\beta1$- and $\beta2$-sheets.

The turn regions in previously reported amyloid structural models are usually not well determined. In the present work, the turn was generated by the CYANA program.[76] During CYANA calculations, the $\beta1$- and $\beta2$-strands were fixed using both distance and dihedral angle restraints with high weights, and the conformation of the turn region was generated randomly by the program. Finally, the turn structure was selected from the resulted pool containing 200 structures by eliminating the ones taking $\alpha$-like conformations or causing intermolecular collapse.

Similar to the above procedure, the inter-protofilament structural model was calculated by docking two $\beta2$-sheets (from two protofilaments of the $\beta1$-turn-$\beta2$ motif which were modeled as described above) through the HADDOCK WeNMR GRID webserver. The Guru interface was used for job submission so that noncrystallographic symmetry restraints between the two $\beta2$-sheets can be defined in the calculation. All observed intermolecular long-range contacts and those used as restraints for HADDOCK calculations of $\beta2-\beta2$ packing are listed in Table S3. All the restraints were duplicated symmetrically between the two $\beta2$-sheets using the same protocol as that used for structural calculations of symmetric dimers. The lower and upper distance cutoffs in the HADDOCK calculation were set to 3.0 and 6.0 Å and to 3.0 and 8.0 Å for short (≤200 ms) and long (400 ms) mixing restraints, respectively. Semi-flexible refinement was enabled on both $\beta2$-sheets.

Since no unambiguous restraints correlating the N-terminal $\beta$-strand ($\beta_N$) to the rest of the peptide have been found, the $\beta_N$ sheet was positioned in several plausible, manually selected orientations. The N-terminal part was also generated and attached to the $\beta$-strand-turn-$\beta$-strand motif in a similar way. Figure 5 was generated using PyMol software.[77]

## RESULTS

**EM Characterization, High-Resolution SSNMR Spectra, and Sequential Assignment.** Recently, several optimized protocols for A$\beta$ sample preparation have been published.[53−55] In this work we took advantage of these new protocols to prepare uniformly [$^{13}$C,$^{15}$N]-labeled A$\beta_{40}$ (with Met0) fibril samples of high molecular homogeneity. The TEM images (Figure 1) reveal that the final product mainly contains bundles of long (>1 $\mu$m) fibrillar material (Figure 1a). The samples contain mainly striated bundles composed by laterally associated filaments (Figure 1b,c). The morphology of "twisted pairs", which were observed in the A$\beta_{40}$ fibrils prepared under quiescent conditions,[19] is not observed in our samples. Moreover, compared with the "striated ribbons" which occur in A$\beta_{40}$ fibrils obtained from gentle agitation,[18] the bundles in our sample (prepared under intensive agitation) seem to lack width modulation along the fibril axis. To the best of our knowledge, such "flat" striated bundles of A$\beta_{40}$ fibrils have not been observed in previous structural studies.[21] The widths of the filaments within the bundles are roughly estimated to be within the range of 3−5 nm (Figure 1d), which is slightly lower than the width of "twisted pairs" (3−8 nm[19]) and similar to those studied in ref 44 (4−6 nm), further suggesting that structural differences could occur between the fibrils obtained within the present work and some previous studies.

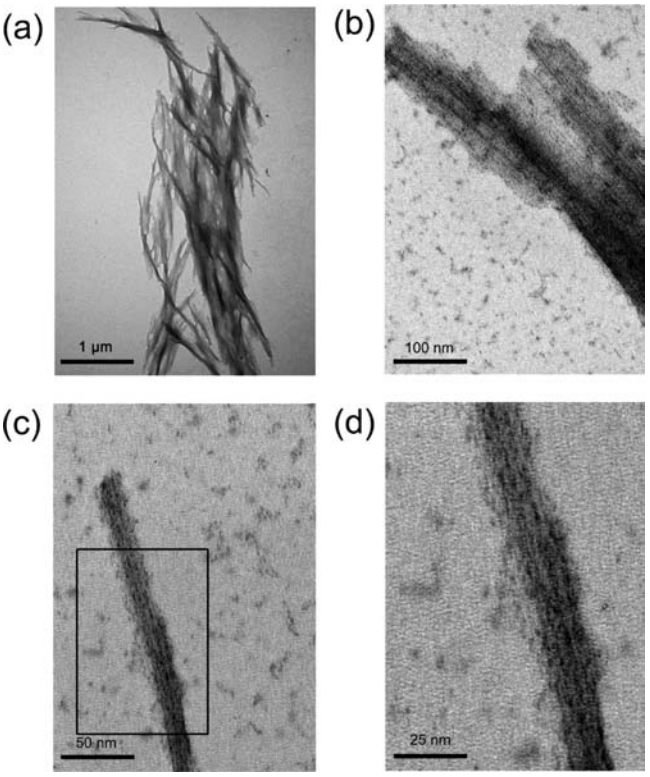


**Figure 1.** TEM images of A$\beta_{40}$ fibrils. (a) A$\beta_{40}$ samples mainly contain mature fibrils. (b) Large bundles of fibrils have been observed. (c) Bundles of fibrils show a striated pattern along the fibril axis. (d) Enlargement of part of (c) permits an estimate of the width of the single fibrils within the bundles of about 3−5 nm.

The SSNMR spectra display well-resolved peaks (Figure 2). The resolved $^{13}C\alpha$ signals are about 90−150 Hz at half-height, which is sensibly smaller than those measured on the well-ordered parts of other A$\beta$ fibrils.[6,19,44,45] By removing homonuclear $J$-coupling ($J_{C\alpha\text{-}C'}$ in this case) by incorporating a S$^3$E scheme into the pulse sequence, the line width of some signals is further reduced by ∼50 Hz. The narrow SSNMR signals are indicators of the high local molecular order. Moreover, single sets of signals are observed for most of the residues, suggesting that the samples contain only one main species. In the NCA spectra (Figure 1b), a weak signal with a $^{15}$N chemical shift of ∼108 ppm may suggest the presence of a minor species, while a small splitting of the signal of Gly25 may suggest the presence of local disorder in the turn region of the $\beta$-strand-turn-$\beta$-strand arrangement discussed below. The quality of the spectra permits, while operating at relatively high magnetic field (16.4−20.0 T) as used in this work, the 2D $^{13}C-^{13}C$ correlation maps to be well resolved. It is worth noting that a polydispersed morphology of fibrils (different fibril lengths and bundle widths) can still be present, while the resolution of the SSNMR spectra is quite high. This has also been noticed on prion fibrils.[39]

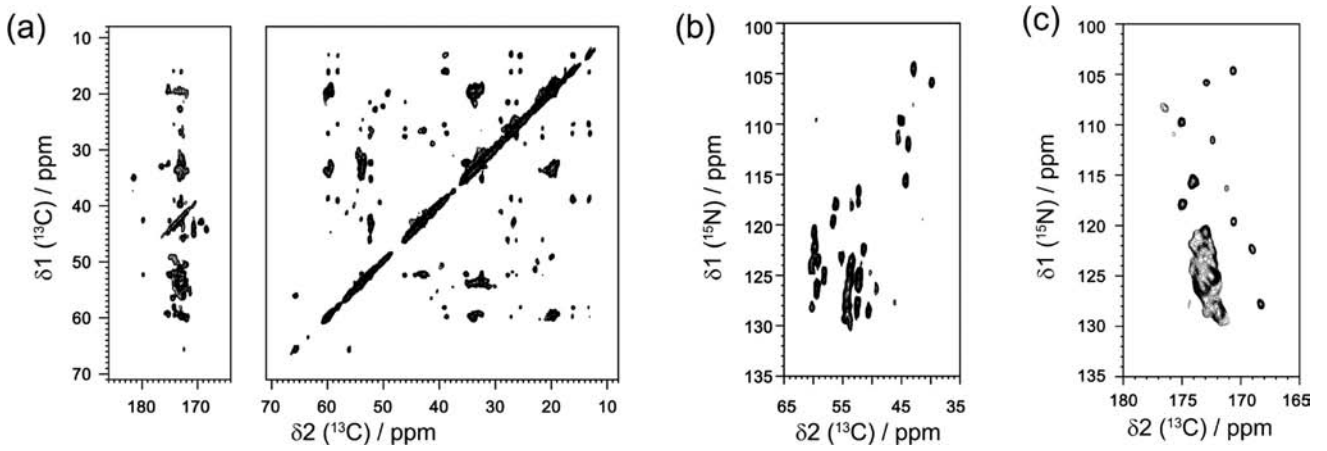


**Figure 2.** SSNMR spectra of uniformly [$^{13}$C,$^{15}$N]-labeled A$\beta_{40}$ fibrils recorded at 14.0 kHz MAS at 20.0 T (850 MHz proton Larmor frequency). (a) Aliphatic−carbonyl and aliphatic−aliphatic regions of the DARR spectra (30 ms mixing time). (b) NCA spectrum. (c) NCO spectrum.

A full sequential assignment can be achieved by the combined analysis of the NCACX, NCOCX, and CANCO spectra (see Materials and Methods for details). Due to the high conformational homogeneity and the high resolution of the spectra, finally all residues but residue 1 and the preceding methionine could be identified in the spectra (Table S1). The signals of Met0 and Asp1 have not been observed, possibly due to local disorder at these two sites, which may broaden the line widths or decrease the intensity of the SSNMR signals. In summary, 39 $^{13}C\alpha$, 39 $^{13}C'$, and 38 backbone $^{15}N$ have been assigned sequentially; 86 out of 114 side-chain $^{13}C$ nuclei from all the 39 assigned residues were also assigned unambiguously. This is, to the best of our knowledge, the most complete assignment of SSNMR spectra of A$\beta$ amyloids to date. The chemical shifts of the assigned residues differ significantly from all the previous reports,[6,19,44,48] indicating structural differences between the present samples and those studied elsewhere.

**Shifted $\beta$-Strand-Turn-$\beta$-Strand Motif in A$\beta_{40}$ Protofilaments.** As shown in Figure 3a, most of the residues in the region Glu11-Val40 display negative secondary chemical shifts ($\Delta\delta$) which are typical reporters of a $\beta$-conformation. Residue Gly25 exhibits a positive $\Delta\delta$ of C$\alpha$, suggesting a break of the $\beta$-strands at and around this site. The TALOS+ program also predicts a high probability of $\beta$-stranded conformation in the regions Glu11-Asp23 and Ile31-Val40 (Figure 3c), in line with the secondary chemical shifts. Residues Gly25 and Ser26 are predicted to have significantly reduced $\beta$-propensity. Taken together, both the $\Delta\delta$ values and the TALOS+ prediction indicate a $\beta$-strand-turn-$\beta$-strand motif (Figure 3b) as found in other A$\beta_{40}$ fibrils.[7,14,18,19,44] The first and second $\beta$-strands in this motif are named $\beta$1 and $\beta$2. The $\beta$1-strand appears longer than usual. Such a long $\beta$-strand has also been recently observed in the PI3-SH3 system.[78]

The organization of the $\beta$-strand-turn-$\beta$-strand motif can be investigated in detail. Signals correlating the side chains of Phe19 and Leu34/Val36 (Figure S1) were detected and assigned unambiguously on the $^{13}C-^{13}C$ DARR/PDSD spectra with 100−400 ms mixing times (Figure S1, Table S2). A detailed analysis of the DARR/PDSD spectra (mixing time 100−1500 ms) provided in total 13 unambiguous as well as 6 ambiguous assignments (Figure S1, Table S2) of long-range contacts. When the long-range unambiguous restraints are drawn on topology models of the $\beta$1-turn-$\beta$2-motifs (Figure 4a−d), it is clear that all these restraints are located in a region which is only consistent with the U-shaped motif shown in Figure 4a. These findings are not compatible with the recent SSNMR studies on A$\beta$ fibrils which show that the phenyl ring of Phe19 is inserted into the space between Ile32 and Leu34 and the side chain of Gln15 is in contact with Val36/Gly37 (Figure 4c).[14,18,19] In the present work, cross peaks between the side chains of Phe19 and Ile32 could not be observed, even using mixing times up to 1500 ms. Moreover, many of the long-range contacts which occur uniquely in other types of $\beta$-strand-turn-$\beta$-strand motif in A$\beta$ fibrils indentified by SSNMR previously (Figure 4b,c)[7,14,44] could not be found in our spectra. Therefore, the structural organization of the U-shaped motif in A$\beta_{40}$ fibrils studied here is distinct from all the previous models.[7,14,18,19,44] Previous SSNMR studies indicate that the polymorphism of A$\beta_{40}$ fibrils is due to different inter-protofilaments interactions, in particular the symmetry characterizing the lateral association of protofilaments.[19] Since the $\beta$-strand-turn-$\beta$-strand motifs are building block of mature fibrils, the observed structural differences at the protofilament level could also be important for the polymorphism of A$\beta_{40}$ fibrils.

Several strategies combining advanced labeling schemes (mixed or diluted sample) and tailored SSNMR methods have been developed to distinguish parallel and antiparallel packing of protein molecules in protofilaments.[18,79,80] In the present study, we have not found any of the cross-peaks that would support an antiparallel packing of the $\beta$1 or $\beta$2 segments in various spectra (PAIN, PAR, and PDSD/DARR) of uniformly labeled samples. In particular, in the region of C$\alpha-$C$\alpha$ (PAR and PDSD/DARR) and N−C$\alpha$ (PAIN), no cross peaks correlating the beginning and ending parts of $\beta$1 or $\beta$2 segments can be assigned in an unambiguous and consistent manner. Therefore, on the basis of such systematic analysis, the $\beta$-strand-turn-$\beta$-strand motifs must be organized in parallel cross-$\beta$ sheets as always found in mature fibrils of A$\beta_{40}$.[14,18,19,44,49] Further evidence supporting the parallel registry of A$\beta$ molecules in the present fibrils can be found in the light of inter-protofilament symmetry considerations (see the next section).

**New Inter-protofilament Interactions in Mature A$\beta_{40}$ Fibrils.** Intense signals correlating the C$\varepsilon$ of Met35 and the C$\gamma$1 of Val39 were found in the DARR spectra with 200 ms mixing time and in the PAR spectra with 10 ms mixing time (Figure S2). These two nuclei are significantly distant from each other (around 9−10 Å) within the $\beta$2-strand of a single molecule,

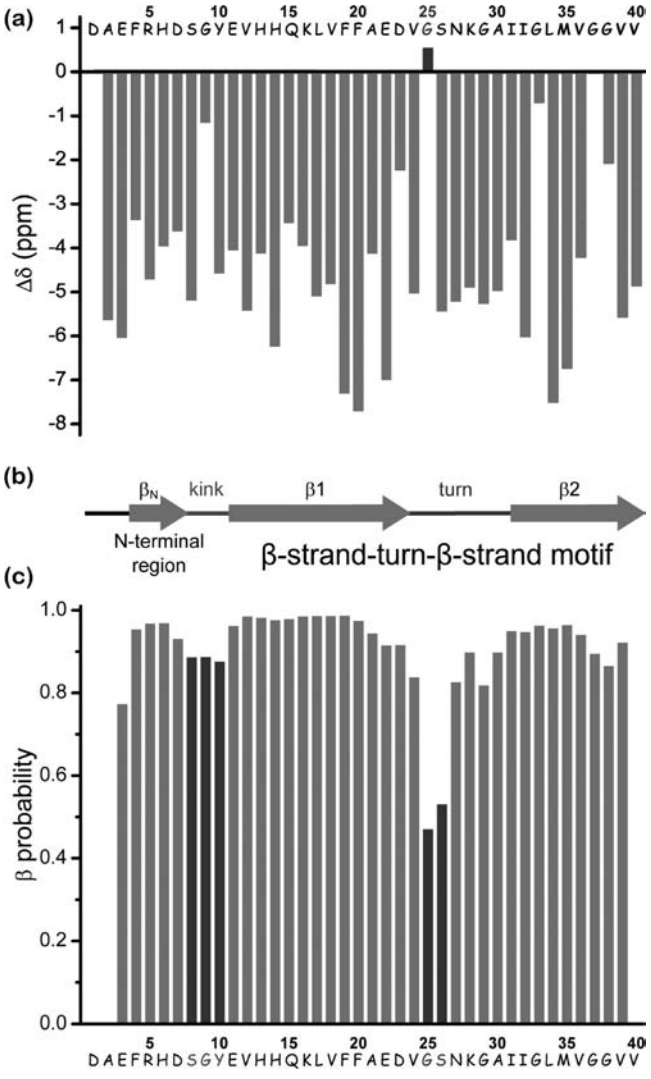


**Figure 3.** Secondary structural analysis of A$\beta_{40}$ fibrils. The residue-specific secondary chemical shifts ($\Delta\delta$) (a) and the TALOS+ predicted $\beta$-probabilities (c) point to the secondary structure elements shown in (b).

and therefore the detected cross peaks linking them in the PDSD spectra must be due to intermolecular contacts. This is further confirmed by several other SSNMR peaks correlating Met35 and the residues (Gly37 and Gly38) close to Val39 (Figure S2, Table S3). These signals indicate that the side chain of Met35 points to the C-terminus of another molecule. Moreover, we have also observed several other long-range contacts linking the starting (Ile31, Ile32, Gly33) and the ending (Val39) parts of the $\beta$2-strands. These latter restraints must also be due to intermolecular contacts and, together with the restraints between Met35 and the ending part of the $\beta$2 strand, point to a $\beta$2-sheet pair with two-fold rotational symmetry (or a so-called co-aligned homozipper,[40] Figure 4e). Such topology has already been proposed to be present in A$\beta_{40}$ fibrils in a previous work[18] and well represents a possible inter-protofilament interface in the present fibrils. As mentioned above, only one single set of SSNMR signals has been observed for most of the residues. As demonstrated in ref 40, within all kinds of protofilament dimers, such an NMR spectral pattern can only occur in the co-aligned homozipper case with a parallel in-registry arrangement of the protofilaments. Therefore, the current observations indeed match the above-mentioned organization of protofilaments as well as the parallel stacking of U-shaped motifs. In other structural models of A$\beta_{40}$ fibrils, the side chain of Met35 is found to be spatially close to the starting part of $\beta$2 (Ile31 of another molecule in dimeric fibrils, Figure 4g)[18,81] or the middle of $\beta$2 (Met35 of another molecule in trimeric fibrils, Figure 4h).[19] Thus, also the structure of the inter-protofilament interface found here is different from the previous reports. It has been demonstrated by previous SSNMR studies that two different morphologies ("striated ribbons" and "twisted pairs") of A$\beta_{40}$ fibrils are directly correlated with the distinct inter-protofilament organizations (Figure 4g,h).[18,19] The A$\beta_{40}$ fibrils ("striated bundles") observed in the present study also show a striated pattern along the fibril axis similar to those observed in the "striated ribbons". This similarity could be linked with the fact that the quaternary structures of the A$\beta_{40}$ fibrils of "striated ribbons" and "striated bundles" share the same two-fold rotational symmetry (Figure 4e,g) in the inter-protofilament organization.

In summary, the U-shaped motif and the protofilament interface share the common structural element $\beta$2. It appears that contacts on the two faces of $\beta$2 ($\beta$1−$\beta$2 contacts in the U-shaped motif and intermolecular $\beta$2−$\beta$2 contacts on the protofilament interface, Figure 4) are both different from previous reports. Indeed, it was observed that a number of $\beta$-stranded amyloid peptide fragments (including one A$\beta$ C-terminal segment), while packed in microcrystals, also experience different inter-$\beta$-strand side-chain contacts on the two faces passing from one crystallographic morphology to another.[8,11] It is reasonable to suggest that the structures of the $\beta$-strand-turn-$\beta$-strand motif and the interprotofilament interface in A$\beta_{40}$ fibrils are linked to one another. The shift of the $\beta$1−$\beta$2 zipper in the U-shaped motif with respect to previous reports is accompanied by a structural adjustment of the initial segment of $\beta$2 around Ile31. The C-terminal region of another peptide molecule could therefore become more adaptive to the intermolecular pairing with the side chain of Met35. This picture is further supported by the observation that in A$\beta_{42}$ fibrils the side chain of Met35 also interacts with the C-terminus region of the other molecules,[14] which is more extended than that in A$\beta_{40}$.

**The N-Terminal Region of A$\beta_{40}$ Fibrils Can Be Structured.** The $\Delta\delta$ values of the N-terminal residues, in particular Phe4-Asp7, are significantly and consecutively negative (Figure 3a). As mentioned above, these are indicators of a $\beta$-stranded conformation. The TALOS+ prediction also points to a high $\beta$-probability on this segment (Figure 3c). Moreover, the overall intensities of the DARR and NCA/NCO signals attributed to the N-terminal residues are close to those of the residues in other well structured parts ($\beta$1 and $\beta$2). Hence the N-terminal part of the peptide in the present fibrils should not experience extensive dynamic disorder, which is expected to diminish the SSNMR signal intensity by averaging out dipolar couplings. On the other hand, static disorder also does not appear to occur in this region, since no obvious broadening and/or multiplication of the SSNMR signals are observed. Therefore, all the present SSNMR data agree with a structured N-terminal region with $\beta$-conformation ($\beta_N$ in Figure 3b) in A$\beta_{40}$ fibrils, which may be also involved in an extended $\beta$-sheet. Despite the present A$\beta_{40}$ construct containing an exogenous N-terminal methionine residue, which might enhance the $\beta$-propensity of the N-terminal part, it is possible that an ordered N-terminal region can be present in wild-type (WT) A$\beta_{40}$ fibrils as well, since a number of studies show that the

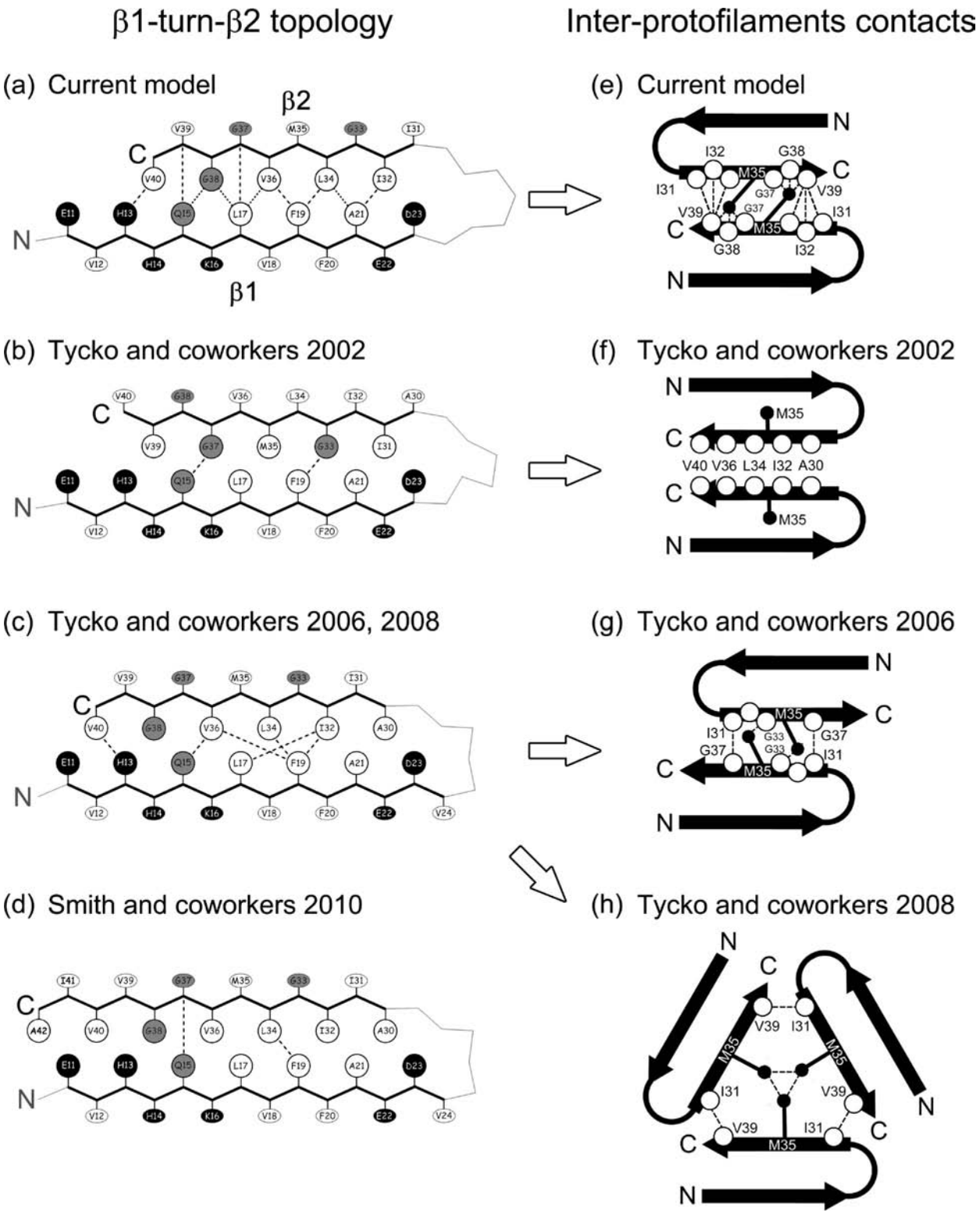


**Figure 4.** Different $\beta$-strand zippers in various SSNMR-derived structural models of A$\beta$ fibrils. The topologies of the $\beta$1-turn-$\beta$2 motif identified in the present work (a) and in other previously studied A$\beta_{40}$ fibrils (b,c)[18,19,44] and A$\beta_{42}$ fibrils (d)[14] are shown in the left column. The dashed/dotted lines represent unambiguous/ambiguous experimental restraints used to derive the corresponding topology. In the schematic description of distinct structures of the U-shaped motif, the hydrophobic, acidic/basic, and other types of residues are shown in white, black, and gray, respectively. The topologies of the interprotofilament interface ($\beta2-\beta2$ zippers) in A$\beta_{40}$ fibrils determined in the present work (e) and proposed previous studies (f–h)[18,19,44] are shown in the right column. The dashed lines represent unambiguous experimental restraints used to derive the corresponding topology. The filled black circles represent the C$\varepsilon$ of the Met35 residue. Other residues included in SSNMR-observed structural restraints for linking the two $\beta$2-strands are shown as hollow circles.


dx.doi.org/10.1021/ja2035859 |J. Am. Chem. Soc. 2011, 133, 16013–16022

present construct has monomer conformation, aggregation kinetics, fibril morphology, and pathological behaviors similar to those of the WT A$\beta_{40}$.[53,82,83]

Our TALOS+ analysis also shows a slight decrease in the $\beta$-propensity of the residues Ser8, Gly9, and Tyr10, suggesting that the conformation of these residues may deviate from the typical $\beta$-conformation. It is therefore possible that the $\beta_N$-strand and the $\beta$1-strand in the U-shaped motif are separated by a short kink (Figure 3b).

Folded N-terminal regions have already been proposed by several recent studies on A$\beta$ fibrils. For example, H/D exchange experiments on certain types of A$\beta_{40}$ fibrils show a considerably low level of solvent exposure in this region, suggesting the presence of a structured N-terminal segment embedded in well-ordered assemblies.[84] In addition, the N-terminal region in recent molecular dynamics (MD) structural models of full-length A$\beta_{42}$ fibrils,[16,85] which are in line with cryo-EM results,[12] also shows a tendency to a $\beta$-conformation. On the other hand, another type of structure—a disordered conformation—was also found on the N-terminal part in some other A$\beta$ fibrils by previous studies based on SSNMR or cryo-EM.[9,18,19,86] Such differences in the structure of the N-terminal regions could be due to the variation of sample preparation conditions, including multiple factors such as the source of A$\beta$ peptides (e.g., synthetic vs recombinant), the purity of samples (e.g., level of residual aggregates), and the fibrillation conditions (e.g., pH, temperature, mechanical force). It can be concluded that the N-terminal part of A$\beta_{40}$ peptides can adopt distinct conformations and thereby also contribute to the structural diversity.

**New Structural Model of A$\beta_{40}$ Fibrils Derived from SSNMR Data.** It has been demonstrated that structural models of A$\beta$ assemblies can be reasonably built based on a few pieces of key structural information.[5,7,14,18,19] In the present work, we capitalize on the fact that all the secondary structural elements ($\beta$1, $\beta$2, and $\beta_N$) have been well identified by chemical shift analysis. This, together with the parallel packing mode revealed by SSNMR data, permits a quick building of the $\beta$1- and, separately, $\beta$2-sheets by duplicating the $\beta$-strands along the fibril axis using conserved interstrand distance (4.7 Å). The use of $\beta$1- and $\beta$2-sheets as the two input "molecules" for the HADDOCK program, rather than the individual $\beta$1- and $\beta$2-strands, dramatically reduces the uncertainty of the calculations by exploiting the efficiency of the surface-recognition algorithm of the program HADDOCK at its best. $\beta$-Sheets composed of an arbitrary number of strands can be employed. In practice, six strands for each of the $\beta$1- and $\beta$2-sheets was found more than sufficient.

A plausible and unique structural model of the A$\beta$ protofilament can therefore be built, both efficiently and with a certain degree of redundancy, through the docking of one $\beta$1-sheet and one $\beta$2-sheet, guided by the nine unambiguous intramolecular long-range restraints per monomer obtained at relatively short mixing times ($\leq$400 ms for DARR/PDSD), listed in boldface in Table S2. With these nine restraints per monomer, the HADDOCK program is already able to converge to a single cluster of 200 structures (see Table S4 for details). Addition of all the other observed intramolecular contacts (unbolded in Table S2), which were not used in the structural calculations because they were either ambiguous or only observed at longer mixing times compared to other restraints, confirmed the structural model and introduced only negligible violations.

In the following step, HADDOCK was used to dock together the two $\beta$2-sheets within two protofilament models using all the intermolecular restraints listed in Table S3. Also in these calculations, a single cluster of 200 structures was obtained (see Table S4 for details). The restraint violations from the HADDOCK calculations are rather low (Table S4), indicating full consistency among these experimental restraints. In summary, the unambiguous long-range restraints found in this work, both intra- and intermolecular, allow the HADDOCK program to pack the $\beta$1−$\beta$2 and the $\beta$2−$\beta$2 zippers in an unambiguous mode. The final model (Figure 5) unambiguously fits all the structural information obtained in this work.

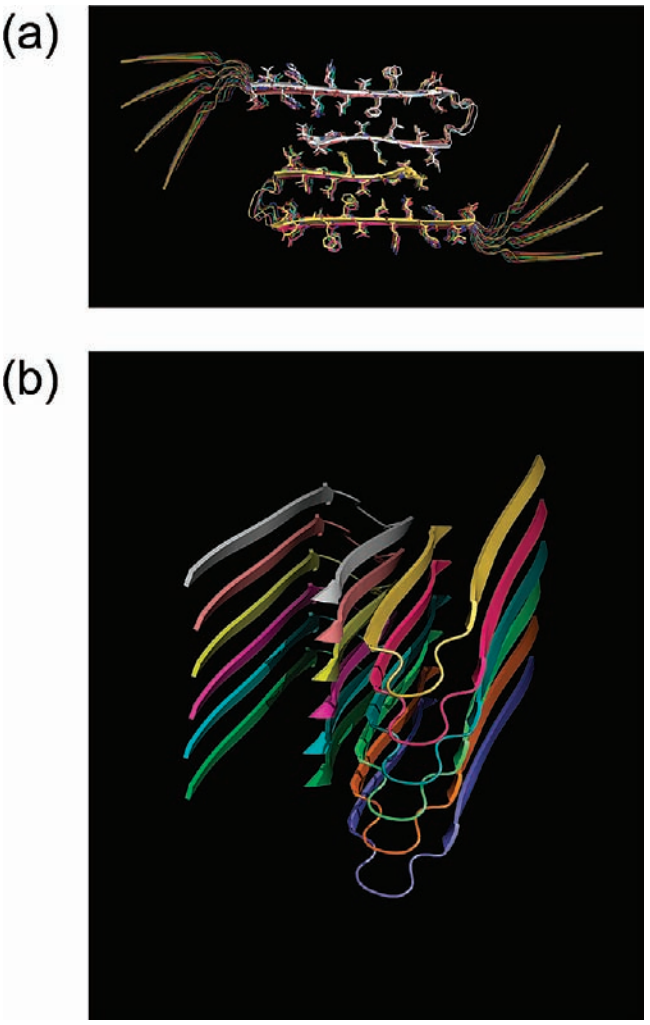


**Figure 5.** A new structural model of A$\beta_{40}$ fibrils. (a) View along the fibril axis illustrating the secondary structure and inter-$\beta$-strand packing ($\beta$1-turn-$\beta$2 motif and dimeric interface). Plausible orientations of the $\beta_N$ strands, which are illustrated as semitransparent parts, are also shown. (b) Side view showing the parallel in-register organization of the molecules along the fibril axis. The N-terminal parts are not shown for clarity.

The thickness of the fibrils in the present structural model along the $\beta$1−$\beta$2−$\beta$2−$\beta$1 direction (zipper direction[40]) is about 4 nm, which is within the estimated width (3−5 nm) of the single filaments in the bundles observed by the present EM imaging, therefore indicating that our structural model is compatible with the EM results.

## DISCUSSION

High-resolution SSNMR studies on fully [$^{13}$C,$^{15}$N]-enriched A$\beta$ fibrils have been hampered for a long time by the broadening

and the multiplication of signals. The sample preparation protocol adopted in this work minimizes the amount of aggregates in the starting material for fibrillation and has been used to produce highly reproducible kinetic data on A$\beta$ aggregation.[53,54] The intensive shaking used here could be a different way to achieve the increase in conformational homogeneity of amyloid fibrils, which was previously obtained by a reseeding process.[19] The improved quality of the samples yields high-resolution SSNMR spectra of fully labeled A$\beta$ fibrils and permits a comprehensive structural study using only uniformly labeled samples. The secondary structures of the A$\beta_{40}$ peptide in this fibrillar form can be analyzed in detail thanks to the availability of the full assignment.

From the new structural model of mature A$\beta_{40}$ fibrils (Figure 5), novel features appear. First, the structure of the inter-protofilament interface within the $\beta2-\beta2$ dimeric architecture could be correlated with the structure of the $\beta1$-turn-$\beta2$ motif by sharing the $\beta2$-strand. Former studies showed that the mutations G33L and G37L lead to failure in forming amyloidal fibrils,[81,87] indicating that they are even able to compromise the structural integrity of the protofilaments. Since they are both located on the outer face of the U-shaped motif, they can only introduce atomic hindrance if a $\beta2-\beta2$ interaction is present. This matches the present finding that, in A$\beta_{40}$ fibrils, the $\beta1$-turn-$\beta2$ folding and the inter-protofilament pairing could be linked. Indeed, the coupling between folding and intermolecular interactions has been observed in many systems involving intrinsically disordered proteins and particularly in the cases where weak hydrophobic interactions dominate the intermolecular recognition.[88] Elaborated mechanisms networking various folding events could exist for guiding the A$\beta$ fibrillation and even for maintaining the structural integrity of mature fibrils.

Second, the structured N-terminal region in fibrils could be functionally important. Several MD calculations suggest that folded A$\beta_{40}$ N-terminal regions could already exist in monomers and even be involved in the initial intermolecular interactions in oligomers that are precursors of mature fibrils.[15,89] Moreover, antibodies targeting the N-terminal region are able to block the formation of A$\beta_{40}$ amyloids.[90] These findings suggest that the N-terminal folding may also contribute to the formation and/or the maturation of A$\beta_{40}$ fibrils. Even more interestingly, several AD-causing mutations are located in the N-terminal segment of A$\beta$.[91,92] These mutations accelerate the fibrillation *in vitro* although they are not in the U-shaped motif which forms the densely packed core of A$\beta$ fibrils. In particular, the A2V and D7N mutations, which are close to the beginning or the end of the $\beta_N$-stretch, increase the $\beta$-propensity, thus suggesting that they may exert pathological effects by primarily enhancing the local folding. Distinct folding states of the N-terminal region were also found in Sc4 and Sc37 amyloids—the two yeast prion strains of Sup35—and are linked to the amyloid stability and functions.[93] The N-terminal region in A$\beta_{40}$ may also be one important factor for the fibril stability and even for its toxicity. It would be interesting to extend the current structural findings on the N-terminal region to other A$\beta$ peptides including the WT construct.

Third, the present results together with other proposed models[18,19,44] underline that the structural diversity of A$\beta_{40}$ fibrils occurs on distinct structural elements and involves various residue sites. It was found that the structural polymorphism of A$\beta_{40}$ fibrils mainly takes place at the supramolecular level.[19] Our work suggests that polymorphism can already originate at the level of the N-terminal conformation, of the zipper of $\beta1$-turn-$\beta2$ motif, and of the inter-protofilament interface. Moreover, both the structure (folding of the N-terminal region, topology of the $\beta1$-turn-$\beta2$ motif and the structure of inter-protofilament interface) and the morphology (striated bundles) of the present fibrils are different from those previously characterized by both SSNMR and EM.[18,19,44] It appears that the structural differences of A$\beta_{40}$ fibrils at the residue/atomic level revealed by high-resolution SSNMR studies (as shown in Figure 4) are somehow correlated with morphological variations at the mesoscopic level demonstrated by EM images. Indeed it is reasonable to speculate that the folding of the monomer and the supramolecular packing (within and between protofilaments) are linked or even define the morphology of amyloid fibrils through the structural duplication/propagation along the fibril axis similar to the growth of 1D nanomaterials. Our structural model is also different from recently proposed models based on cryo-EM measurements,[21] further showing the high degree of complexity in the structural polymorphisms of A$\beta$ fibrils.

In summary, the present results show that site-specific as well as high-order structural information on A$\beta$ fibrils can be obtained using only uniformly [$^{13}$C,$^{15}$N]-labeled samples. This permits a structural study of both the monomer folding and the supramolecular packing at high resolution. With SSNMR-data-derived knowledge on secondary structure and registry mode of the molecules within the protofilament, a structural model of amyloid fibrils can be reliably obtained through docking $\beta$-spines using experimental restraints. This work leads to the structural identification of a new type of mature A$\beta_{40}$ fibrils and provides valuable information toward the understanding of amyloid polymorphism at atomic resolution.

## ■ ASSOCIATED CONTENT

**Supporting Information.** More-detailed technical description of the solid-state NMR experiments, assigned $^{13}$C and $^{15}$N resonances of A$\beta_{40}$ fibrils, assigned long-range restraints, structural statistics of HADDOCK calculations, the schematic representation of the assignment of the long-range contacts, and complete ref 91. This material is available free of charge via the Internet at http://pubs.acs.org.

## ■ AUTHOR INFORMATION

**Corresponding Author**
ivanobertini@cerm.unifi.it; luchinat@cerm.unifi.it

## ■ ACKNOWLEDGMENT

The WeNMR project (European FP7 e-Infrastructure grant, contract no. 261572, http://www.wenmr.eu), the Bio-NMR project (European FP7 e-Infrastructure grant, contract no. 261863, http://www.bio-nmr.net/, Working Package 20), INSTRUCT (European FP7 e-Infrastructure grant, contract no. 211252, http://www.instruct-fp7.eu/), and Ente Cassa Risparmio Firenze are acknowledged for financial support. Dr. Moreno Lelli is acknowledged for kind help with the initial NMR experiments and highly valuable discussions. We thank the Centro di Microscopie Elettroniche (CNR di Firenze) for help with the TEM tests.

## ■ REFERENCES

(1) Querfurth, H. W.; LaFerla, F. M. *N. Engl. J. Med.* **2010**, *362*, 329–344.

(2) Lee, S. J.; Desplats, P.; Sigurdson, C.; Tsigelny, I.; Masliah, E. *Nat. Rev. Neurol.* **2010**, *6*, 702–706.
(3) Haass, C. *Nat. Med.* **2010**, *16*, 1201–1204.
(4) Teller, J. K.; Russo, C.; Debusk, L. M.; Angelini, G.; Zaccheo, D.; DagnaBricarelli, F.; Scartezzini, P.; Bertolini, S.; Mann, D. M. A.; Tabaton, M.; Gambetti, P. *Nat. Med.* **1996**, *2*, 93–95.
(5) Luhrs, T.; Ritter, C.; Adrian, M.; Riek-Loher, D.; Bohrmann, B.; Doeli, H.; Schubert, D.; Riek, R. *Proc. Natl. Acad. Sci. U.S.A.* **2005**, *102*, 17342–17347.
(6) Petkova, A. T.; Leapman, R. D.; Guo, Z. H.; Yau, W. M.; Mattson, M. P.; Tycko, R. *Science* **2005**, *307*, 262–265.
(7) Chimon, S.; Shaibat, M. A.; Jones, C. R.; Calero, D. C.; Aizezi, B.; Ishii, Y. *Nat. Struct. Mol. Biol.* **2007**, *14*, 1157–1164.
(8) Sawaya, M. R.; Sambashivan, S.; Nelson, R.; Ivanova, M. I.; Sievers, S. A.; Apostol, M. I.; Thompson, M. J.; Balbirnie, M.; Wiltzius, J. J. W.; McFarlane, H. T.; Madsen, A. O.; Riekel, C.; Eisenberg, D. *Nature* **2007**, *447*, 453–457.
(9) Sachse, C.; Fandrich, M.; Grigorieff, N. *Proc. Natl. Acad. Sci. U.S.A.* **2008**, *105*, 7462–7466.
(10) Peralvarez-Marin, A.; Barth, A.; Graslund, A. *J. Mol. Biol.* **2008**, *379*, 589–596.
(11) Wiltzius, J. J. W.; Landau, M.; Nelson, R.; Sawaya, M. R.; Apostol, M. I.; Goldschmidt, L.; Soriaga, A. B.; Cascio, D.; Rajashankar, K.; Eisenberg, D. *Nat. Struct. Mol. Biol.* **2009**, *16*, 973–978.
(12) Zhang, R.; Hu, X. Y.; Khant, H.; Ludtke, S. J.; Chiu, W.; Schmid, M. F.; Frieden, C.; Lee, J. M. *Proc. Natl. Acad. Sci. U.S.A.* **2009**, *106*, 4653–4658.
(13) Schmidt, M.; Sachse, C.; Richter, W.; Xu, C.; Fandrich, M.; Grigorieff, N. *Proc. Natl. Acad. Sci. U.S.A.* **2009**, *106*, 19813–19818.
(14) Ahmed, M.; Davis, J.; Aucoin, D.; Sato, T.; Ahuja, S.; Aimoto, S.; Elliott, J. I.; Van Nostrand, W. E.; Smith, S. O. *Nat. Struct. Mol. Biol.* **2010**, *17*, 561–567.
(15) Urbanc, B.; Betnel, M.; Cruz, L.; Bitan, G.; Teplow, D. B. *J. Am. Chem. Soc.* **2010**, *132*, 4266–4280.
(16) Miller, Y.; Ma, B.; Nussinov, R. *J. Am. Chem. Soc.* **2011**, *133*, 2742–2748.
(17) Linser, R.; Dasari, M.; Hiller, M.; Higman, V.; Fink, U.; del Amo, J.-M. L.; Markovic, S.; Handel, L.; Kessler, B.; Schmieder, P.; Oesterhelt, D.; Oschkinat, H.; Reif, B. *Angew. Chem., Int. Ed.* **2011**, *50*, 4508–4512.
(18) Petkova, A. T.; Yau, W. M.; Tycko, R. *Biochemistry* **2006**, *45*, 498–512.
(19) Paravastu, A. K.; Leapman, R. D.; Yau, W. M.; Tycko, R. *Proc. Natl. Acad. Sci. U.S.A.* **2008**, *105*, 18349–18354.
(20) Meinhardt, J.; Sachse, C.; Hortschansky, P.; Grigorieff, N.; Fandrich, M. *J. Mol. Biol.* **2009**, *386*, 869–877.
(21) Fandrich, M.; Schmidt, M.; Grigorieff, N. *Trends Biochem. Sci.* **2011**, *36*, 338–345.
(22) Debelouchina, G. T.; Platt, G. W.; Bayro, M. J.; Radford, S. E.; Griffin, R. G. *J. Am. Chem. Soc.* **2010**, *132*, 10414–10423.
(23) Van der Wel, P. C. A.; Lewandowski, J. R.; Griffin, R. G. *Biochemistry* **2010**, *49*, 9457–9469.
(24) Lewandowski, J. R.; van der Wel, P. C.A.; Rigney, M.; Grigorieff, N.; Griffin, R. G. *J. Am. Chem. Soc.* **2011**, *133*, 14686–14698.
(25) Paravastu, A. K.; Petkova, A. T.; Tycko, R. *Biophys. J.* **2006**, *90*, 4618–4629.
(26) Paravastu, A. K.; Qahwash, I.; Leapman, R. D.; Meredith, S. C.; Tycko, R. *Proc. Natl. Acad. Sci. U.S.A.* **2009**, *106*, 7443–7448.
(27) Miller, Y.; Ma, B.; Nussinov, R. *Chem. Rev.* **2010**, *110*, 4820–4838.
(28) Renault, M.; Cukkemane, A.; Baldus, M. *Angew. Chem., Int. Ed.* **2010**, *49*, 8346–8357.
(29) Castellani, F.; van Rossum, B.; Diehl, A.; Schubert, M.; Rehbein, K.; Oschkinat, H. *Nature* **2002**, *420*, 98–102.
(30) Lange, A.; Giller, K.; Hornig, S.; Martin-Eauclaire, M. F.; Pongs, O.; Becker, S.; Baldus, M. *Nature* **2006**, *440*, 959–962.
(31) Cady, S. D.; Schmidt-Rohr, K.; Wang, J.; Soto, C. S.; DeGrado, W. F.; Hong, M. *Nature* **2010**, *463*, 689–692.
(32) Sharma, M.; Yi, M. G.; Dong, H.; Qin, H. J.; Peterson, E.; Busath, D. D.; Zhou, H. X.; Cross, T. A. *Science* **2010**, *330*, 509–512.
(33) Jehle, S.; Rajagopal, P.; Bardiaux, B.; Markovic, S.; Kuhne, R.; Stout, J. R.; Higman, V. A.; Klevit, R. E.; van Rossum, B. J.; Oschkinat, H. *Nat. Struct. Mol. Biol.* **2010**, *17*, 1037–1042.
(34) Ader, C.; Frey, S.; Maas, W.; Schmidt, H. B.; Gorlich, D.; Baldus, M. *Proc. Natl. Acad. Sci. U.S.A.* **2010**, *107*, 6281–6285.
(35) Jaroniec, C. P.; MacPhee, C. E.; Bajaj, V. S.; McMahon, M. T.; Dobson, C. M.; Griffin, R. G. *Proc. Natl. Acad. Sci. U.S.A.* **2004**, *101*, 711–716.
(36) Heise, H.; Hoyer, W.; Becker, S.; Andronesi, O. C.; Riedel, D.; Baldus, M. *Proc. Natl. Acad. Sci. U.S.A.* **2005**, *102*, 15871–15876.
(37) Ferguson, N.; Becker, J.; Tidow, H.; Tremmel, S.; Sharpe, T. D.; Krause, G.; Flinders, J.; Petrovich, M.; Berriman, J.; Oschkinat, H.; Fersht, A. R. *Proc. Natl. Acad. Sci. U.S.A.* **2006**, *103*, 16248–16253.
(38) Iwata, K.; Fujiwara, T.; Matsuki, Y.; Akutsu, H.; Takahashi, S.; Naiki, H.; Goto, Y. *Proc. Natl. Acad. Sci. U.S.A.* **2006**, *103*, 18119–18124.
(39) Wasmer, C.; Lange, A.; Van Melckebeke, H.; Siemer, A. B.; Riek, R.; Meier, B. H. *Science* **2008**, *319*, 1523–1526.
(40) Nielsen, J. T.; Bjerring, M.; Jeppesen, M. D.; Pedersen, R. O.; Pedersen, J. M.; Hein, K. L.; Vosegaard, T.; Skrydstrup, T.; Otzen, D. E.; Nielsen, N. C. *Angew. Chem., Int. Ed.* **2009**, *48*, 2118–2121.
(41) Barbet-Massin, E.; Ricagno, S.; Lewandowski, J. R.; Giorgetti, S.; Bellotti, V.; Bolognesi, M.; Emsley, L.; Pintacuda, G. *J. Am. Chem. Soc.* **2010**, *132*, 5556–5557.
(42) Debelouchina, G. T.; Platt, G. W.; Bayro, M. J.; Radford, S. E.; Griffin, R. G. *J. Am. Chem. Soc.* **2010**, *132*, 10414–10423.
(43) Tycko, R. *Q. Rev. Biophys.* **2006**, *39*, 1–55.
(44) Petkova, A. T.; Ishii, Y.; Balbach, J. J.; Antzutkin, O. N.; Leapman, R. D.; Delaglio, F.; Tycko, R. *Proc. Natl. Acad. Sci. U.S.A.* **2002**, *99*, 16742–16747.
(45) Tycko, R.; Ishii, Y. *J. Am. Chem. Soc.* **2003**, *125*, 6606–6607.
(46) Chimon, S.; Ishii, Y. *J. Am. Chem. Soc.* **2005**, *127*, 13472–13473.
(47) Scheidt, H. A.; Morgado, I.; Rothemund, S.; Huster, D.; Fändrich, M. *Angew. Chem., Int. Ed.* **2011**, *50*, 2837–2840.
(48) Parthasarathy, S.; Long, F.; Miller, Y.; Xiao, Y.; McElheny, D.; Thurber, K.; Ma, B.; Nussinov, R.; Ishii, Y. *J. Am. Chem. Soc.* **2011**, *133*, 3390–3400.
(49) Qiang, W.; Yau, W.-M.; Tycko, R. *J. Am. Chem. Soc.* **2011**, *133*, 4018–4029.
(50) Roher, A. E.; Lowenson, J. D.; Clarke, S.; Woods, A. S.; Cotter, R. J.; Gowing, E.; Ball, M. J. *Proc. Natl. Acad. Sci. U.S.A.* **1993**, *90*, 10836–10840.
(51) Naslund, J.; Schierhorn, A.; Hellman, U.; Lannfelt, L.; Roses, A. D.; Tjernberg, L. O.; Silberring, J.; Gandy, S. E.; Winblad, B.; Greengard, P.; Nordstedt, C.; Terenius, L. *Proc. Natl. Acad. Sci. U.S.A.* **1994**, *91*, 8378–8382.
(52) Cirrito, J. R.; May, P. C.; O'Dell, M. A.; Taylor, J. W.; Parsadanian, M.; Cramer, J. W.; Audia, J. E.; Nissen, J. S.; Bales, K. R.; Paul, S. M.; DeMattos, R. B.; Holtzman, D. M. *J. Neurosci.* **2003**, *23*, 8844–8853.
(53) Walsh, D. M.; Thulin, E.; Minogue, A. M.; Gustavsson, N.; Pang, E.; Teplow, D. B.; Linse, S. *FEBS J.* **2009**, *276*, 1266–1281.
(54) Hellstrand, E.; Boland, B.; Walsh, D. M.; Linse, S. *ACS Chem. Neurosci.* **2010**, *1*, 13–18.
(55) Jan, A.; Hartley, D. M.; Lashuel, H. A. *Nat. Protoc.* **2010**, *5*, 1186–1209.
(56) Takegoshi, K.; Nakamura, S.; Terao, T. *Chem. Phys. Lett.* **2001**, *344*, 631–637.
(57) Takegoshi, K.; Nakamura, S.; Terao, T. *J. Chem. Phys.* **2003**, *118*, 2325–2341.
(58) Lewandowski, J. R.; De Paepe, G.; Griffin, R. G. *J. Am. Chem. Soc.* **2007**, *129*, 728–729.
(59) Paëpe, D. G.; Lewandowski, J. R.; Loquet, A.; Eddy, M.; Megy, S.; Böckmann, A.; Griffin, R. G. *J. Chem. Phys.* **2011**, *134*, 095101.
(60) Baldus, M.; Petkova, A. T.; Herzfeld, J.; Griffin, R. G. *Mol. Phys.* **1998**, *95*, 1197–1207.

(61) Pauli, J.; Baldus, M.; van Rossum, B.; de Groot, H.; Oschkinat, H. *ChemBioChem* **2001**, *2*, 272–281.
(62) Castellani, F.; van Rossum, B. J.; Diehl, A.; Rehbein, K.; Oschkinat, H. *Biochemistry* **2003**, *42*, 11476–11483.
(63) Li, Y.; Berthold, D. A.; Frericks, H. L.; Gennis, R. B.; Rienstra, C. M. *ChemBioChem* **2007**, *8*, 434–442.
(64) Bjerring, M.; Nielsen, A. B.; Tosner, Z.; Nielsen, N. C. *Chem. Phys. Lett.* **2010**, *494*, 326–330.
(65) Bloembergen, N. *Physica* **1949**, *15*, 386–426.
(66) Laage, S.; Lesage, A.; Emsley, L.; Bertini, I.; Felli, I. C.; Pierattelli, R.; Pintacuda, G. *J. Am. Chem. Soc.* **2009**, *131*, 10816–10817.
(67) De Paepe, G.; Lewandowski, J. R.; Loquet, A.; Bockmann, A.; Griffin, R. G. *J. Chem. Phys.* **2008**, *129*, 245101.
(68) Lewandowski, J. R.; De Paepe, G.; Eddy, M. T.; Struppe, J.; Maas, W.; Griffin, R. G. *J. Phys. Chem. B* **2009**, *113*, 9062–9069.
(69) (a) Keller, R. *The Computer Aided Resonance Assignment Tutorial*; CANTINA Verlag: Goldau, Switzerland, 2004. (b) Keller, R. Ph.D. thesis, Diss. ETH Nr. 15947, The Swiss Federal Institute of Technology, Zürich, 2004. The CARA software was downloaded from http://cara.nmr.ch/doku.php/home.
(70) Goddard, D. T.; Kneller, G. D. *SPARKY*, 2007.
(71) Luca, S.; Filippov, D. V.; Van Boom, J. H.; Oschkinat, H.; de Groot, H. J. M.; Baldus, M. *J. Biomol. NMR* **2001**, *20*, 325–331.
(72) Shen, Y.; Delaglio, F.; Cornilescu, G.; Bax, A. *J. Biomol. NMR* **2009**, *44*, 213–223.
(73) Dominguez, C.; Boelens, R.; Bonvin, A. M. J. J. *J. Am. Chem. Soc.* **2003**, *125*, 1731–1737.
(74) de Vries, S. J.; van Dijk, A. D. J.; Krzeminski, M.; van Dijk, M.; Thureau, A.; Hsu, V.; Wassenaar, T.; Bonvin, A. M. J. J. *Proteins Struct., Funct. Bioinf.* **2007**, *69*, 726–733.
(75) de Vries, S. J.; van Dijk, M.; Bonvin, A. M. J. J. *Nat. Protoc.* **2010**, *5*, 883–897.
(76) Guntert, P.; Mumenthaler, C.; Wuthrich, K. *J. Mol. Biol.* **1997**, *273*, 283–298.
(77) DeLano, W. L. *The PyMOL Molecular Graphics System*; DeLano Scientific: San Carlos, CA, 2002; http://www.pymol.org.
(78) Bayro, M. J.; Maly, T.; Birkett, N. R.; MacPhee, C. E.; Dobson, C. M.; Griffin, R. G. *Biochemistry* **2010**, *49*, 7474–7484.
(79) Loquet, A.; Giller, K.; Becker, S.; Lange, A. *J. Am. Chem. Soc.* **2010**, *132*, 15164–15166.
(80) Bayro, M. J.; Debelouchina, G. T.; Eddy, M. T.; Birkett, N. R.; MacPhee, C. E.; Rosay, M. M.; Maas, W. E.; Dobson, C. M.; Griffin, R. G. *J. Am. Chem. Soc.* 2011, *133*, 13967–13974.
(81) Sato, T.; Kienlen-Campard, P.; Ahmed, M.; Liu, W.; Li, H. L.; Elliott, J. I.; Aimoto, S.; Constantinescu, S. N.; Octave, J. N.; Smith, S. O. *Biochemistry* **2006**, *45*, 5503–5516.
(82) Macao, B.; Hoyer, W.; Sandberg, A.; Brorsson, A. C.; Dobson, C. M.; Hard, T. *BMC Biotechnol.* **2008**, *8*, 82.
(83) Luheshi, L. M.; Hoyer, W.; de Barros, T. P.; Hard, I. V.; Brorsson, A. C.; Macao, B.; Persson, C.; Crowther, D. C.; Lomas, D. A.; Stahl, S.; Dobson, C. M.; Hard, T. *PLOS Biol.* **2010**, *8*, e1000334.
(84) Kodali, R.; Williams, A. D.; Chemuru, S.; Wetzel, R. *J. Mol. Biol.* **2010**, *401*, 503–517.
(85) Miller, Y.; Ma, B. Y.; Tsai, C. J.; Nussinov, R. *Proc. Natl. Acad. Sci. U.S.A.* **2010**, *107*, 14128–14133.
(86) Sachse, C.; Grigorieff, N.; Fandrich, M. *Angew. Chem., Int. Ed.* **2010**, *49*, 1321–1323.
(87) Kim, S.; Jeon, T. J.; Oberai, A.; Yang, D.; Schmidt, J. J.; Bowie, J. U. *Proc. Natl. Acad. Sci. U.S.A.* **2005**, *102*, 14278–14283.
(88) Sugase, K.; Dyson, H. J.; Wright, P. E. *Nature* **2007**, *447*, 1021–1025.
(89) Lam, A. R.; Teplow, D. B.; Stanley, H. E.; Urbanc, B. *J. Am. Chem. Soc.* **2008**, *130*, 17413–17422.
(90) Gardberg, A. S.; Dice, L. T.; Ou, S.; Rich, R. L.; Heimbrecht, E.; Ko, J.; Wetzel, R.; Myszka, D. G.; Patterson, P. H.; Dealwis, C. *Proc. Natl. Acad. Sci. U.S.A.* **2007**, *104*, 15659–15664.
(91) Di Fede, G.; et al. *Science* **2009**, *323*, 1473–1477.
(92) Ono, K.; Condron, M. M.; Teplow, D. B. *J. Biol. Chem.* **2010**, *285*, 23184–23195.
(93) Toyama, B. H.; Kelly, M. J. S.; Gross, J. D.; Weissman, J. S. *Nature* **2007**, *449*, 233–237.